

Efficient Procedure and Methods to Determine Critical Electroporation Parameters

Gaddi Blumrosen[‡], Alireza Abazari[‡], Alexander Golberg[‡], Mehmet Tonner, and Martin L. Yarmush

Abstract— Controlling electroporation and determination of its design parameters govern the performance in many electroporation applications in the fields of medicine, biology, and food industry. This work provides an enhanced high throughput signal processing method to enable non-expert, objective, automatic and fast analysis of large datasets of microscopic images of high throughput electroporation experiments. This can enable optimal design of vital electroporation parameters including the optimal thresholds for the electric field strength, and the optimal number of pulses. In this work the non-expert visualization platform and the methods are described, and implemented on normal dermal human fibroblasts cell culture.

Index Terms— Electroporation, clustering, Image processing, Light Microscopy, Biological system modeling.

I. INTRODUCTION

ELECTROPORATION is inducing cell membrane permeabilisation (poration) by applying an external, high voltage, short-pulsed electrical field [1]. If the permeabilisation is temporary and the membrane reseals after removing the field, the procedure is called reversible electroporation; if the membrane does not reseal (eventually followed by cell death), the procedure is called irreversible electroporation. Electroporation is used for different applications in medicine, biotechnology and food industry [2],[3]. The medical and biotechnology applications of electroporation began in 1982 with the work of Neumann and colleagues [4]. The authors used pulsed electric fields to temporarily permeabilize a cell membrane to deliver a foreign DNA into cells. In the following decade, the combination of high voltage pulsed electric fields with the chemotherapeutic drugs and DNA emerged into novel clinical applications

named electro-chemotherapy [5-7] and gene electro-transfer [8,9], respectively. In the past decade, non-thermal irreversible electroporation for the ablation of solid tumors has emerged as a new medical application of electroporation technology [3, 10]. In the food and pharmaceutical application, electroporation is used for bacterial disinfection [2,11].

The successful electroporation procedure is predicated by the cell properties, cell environment and the applied electric fields. The main properties of the cells which affect the electroporation are cell size, shape, membrane structure, and surface charge [2], [12]. The electric field properties which affect the electroporation procedure are the pulse intensity, number of pulses, pulse duration, pulse shape, and frequency [2]. Studies in the last three decades show that electroporation occurs after the applied electric field reaches a certain value called electroporation threshold. In addition, at the specific applied electric field, there is a threshold for the number of pulses and pulse length, which are required for effective electroporation procedure [13]. Defining the specific electroporation parameters for specific cells types in the specific environment is an elaborate and time consuming task. Currently, an electroporation user needs to apply a long tedious, inaccurate, series of experiments to identify the effects of electric field intensity, number of pulses and pulse duration impact on the efficacy of electroporation procedures. For each parameter a series of separate experiments are needed [13], which is a time consuming tedious task.

Currently, the main existing problems in the field of electroporation are: 1) there is no analytical expression that can accurately predict the effect of the electroporation-induced mass transport in the cell population; 2) the existing verification processes are not automatic and require an expert to extract information; 3) no objective tools exist for the determination of critical electroporation parameters, which leads to inaccurate treatment, and loss of critical time and large variation in the electroporation protocols; 4) the development of automated microscopes in recent years has turned microscopy into a predominantly quantitative technique [15]. Still, the high resolution images are huge in size, and require an expert to view the images. Furthermore, there is a need to compress this huge amount of data to objective informative measure.

Recently, a high-throughput experimental method for determining irreversible electroporation electric field strength threshold using concentric electrodes design was suggested in [14]. A co-centric electrode configuration that allows

The white paper was submitted on 28.12.2013. This work was supported in part by Shriners Grant #85120-BOS.

G. B. (corresponding author) is with the computer science department in Tel Aviv University, Tel Aviv, Israel (gaddi.b@gmail.com).

A. G. and A.A., M.T. and M. L. Y are with the Center for Engineering in Medicine, Department of Surgery, Massachusetts General Hospital, Harvard Medical School, and Shriners Burns Institute, Boston, MA 02114, USA. M. L.Y. is also with Department of Biomedical Engineering, Rutgers University, Piscataway, NJ 08854.

[‡]*equal contributors*

screening of multiple electric fields in the same experiment was suggested in this work. It can assist in determination of the irreversible electroporation threshold. However, it does not provide a computational platform to characterize time-dependent mass transport associated with reversible electroporation phenomena, which is crucially important for the accurate treatment planning of the electro-chemotherapy. Furthermore, the work in [14], does not provide sufficient methods that can extract the electroporation parameters in automatic manner.

The main goal of this paper is to suggest an experimental procedure that extend the work in [14], and give the supporting processing methods, that enable non-expert electroporation users to derive the required parameters for the desired electroporation application, with minimal resources. The suggested procedure accompanied by an analytic tools and visualization platforms can provide easy way for non-expert electroporation users like physicians and biologists without strong technological background to evaluate the effect of the electroporation on their cell target, and rapidly tailor the electroporation performance to their needs. This work extend the work in

The paper is organized as follows. In section II, the model for electroporation effect on cells' culture is presented. In Section III, the analytical methods tailored to the fluorescent cells' culture are derived. Section IV, presents the results, and the visualization methods of the software utility we derived, and in Section V, we conclude the work, and give future work.

II. MODELING ELECTROPORATION EFFECT ON CELLS' CULTURE

Our suggested procedure is based on measuring the loss of fluorescence intensity from pre-stained cells after electroporation in a fluorophore-free medium. The fluorescent stain consists of fluorophore molecules, which are freely floating in the cytoplasm of the cell and are not binding to any specific cell protein/organelles. The fluorophore molecules also cannot penetrate the cell membrane unless assisted by pore formation due to electroporation. Immediately after the electric field is removed, the intracellular fluorophore molecules flow through the pores to the surrounding medium due to concentration gradient. The diffusion equation that describes the change in the intracellular concentration of fluorophores in each cell [16] is:

$$\frac{dC}{dt} = -P \frac{\phi A_{cell}}{V_{cell}} (C - C^*), \quad (1)$$

where C the concentration of the fluorescent molecule inside the cell, C^* is the extracellular concentration of the fluorophore (assumed equal to zero at all times), A_{cell} and V_{cell} are the total cell area and volume, and are constants. With our definition, P is the membrane permeability through the open area and ϕ is the area fraction of the pores that form due to the electrical field.

In human cell culture, the cell area and volumes change from cell to cell. Furthermore, there is variability in the cell permeability P , due to the variability in cell membrane composition. In addition, ϕ depends on the strength of the

electrical field, and vary between each cell and changes over time. Stronger electroporation leads to larger flux of molecules out of the cells. In irreversible electroporation, the area fraction of the pores, μ , will reach after certain time from the end of electroporation treatment, to a certain constant level. In reversible electroporation, in the other hand, the cell pores area get smaller, as some of the pores get closed after certain time, which leads to decrease in its value.

Solving (1) involves solving nonlinear models of the cell membrane, with inaccurate parameter estimations such as membrane permeability constant, and the area fraction of the pores [17, 18], and thus is very sensitive to model errors. Thus, deriving an analytical solution to cell culture must include statistical assumptions for large-scale model, and require relying on some level on experimental of the specific culture cell results [19].

The proposed electroporation system consists of the cell type of interest cultured on a disk, with two electrodes, where one (the cathode) is positioned at the center of the disk, and the other (the anode), on radius R_2 , as shown in Figure 1. The cell culture sits between the two spherical electrodes locations, R_1 , and R_2 , $R_1 < r < R_2$. For microscope imaging of electroporation driven mass transports, the cells are loaded with a fluorescent stain. We assume that the molecules that exit the cell will never flow in and thus can be seen as if they have been removed from the system.

The electric field distribution, to which cells are exposed in the concentric electrode design, used in this study is:

$$E(r) = \frac{V_1 - V_2}{r \ln(R_2/R_1)}, \quad (2)$$

where V_1 , and V_2 , are the voltage at ranges of R_1 , and R_2 , respectively. At each radius r , the cells will be exposed to a location specific electric field, $E(r)$.

This experimental methodology, allows screening the effect of multiple electric fields at one experiment, and consequently enables faster identification of critical electroporation parameters than what was used.

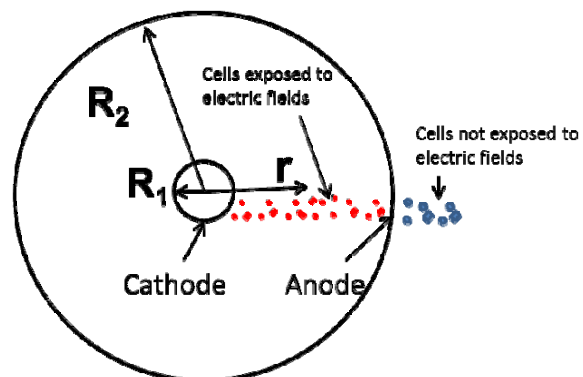


Fig. 1. describes the positioning of the cell culture and of the two spherical electrodes, at locations, R_1 (the cathode) and R_2 (the anode). The electrical field induced between the two electrodes (cathode and anode) is radial, and decreases over the distance from the cathode. The cells' culture of interest is located in between the cathode and the anode.

III. PROCESSING METHODS

Let's define the intensity of a cell at instance time i , and location r along the radius as $I_{i,r}^{cell}$. In this work we assume that intensity is directly related to the concentration of fluorescent material inside the cell.

The focus of this work will be on cells along the one dimensional radius of the line along that connects between the anode and cathode locations, $R_1 < r < R_2$. We will examine a strip along the radius, of length L , where $L > r_{cell}$, so there will be at least few cells in the strip width.

The electroporation area governed by r_e , will be quantized to N , $N = \frac{|R_2 - R_1|}{L_r}$, forming N blocks of size $L \times L_r$ pixels. The block range dimension L_r , is chosen in a way that it captures enough cell to give sufficient statistics, and yet that the electrical field in the block is relatively constant (quasi-static assumption). In the experiment we will examine N time instances that assumed to be enough to capture the full electroporation effect, after the end of the pulses. As a reference point, an area, outside of the electroporation range, will be used to exclude temporal artifacts, caused by possible changes in illuminations or material leakage during the experiments.

The methods can be divided into two parts: estimating the intracellular fluorescent molecule concentration as a function of electric field exposure parameters and post-exposure time. The first part include pre-processing of the images, tracking over time and range over the cell concentration, and then post processing to exclude spatial-temporal artifacts. The second part includes registration the fundamental electroporation parameters of effective treatment range, and the required number of pulses.

A. Estimating concentration of fluorescent material in time and at different electrical field level along the radius

First, the images from the microscopy at different slices are stitched, and aligned in case the disks moves and excluding part of the images those are not overlapping.

Cell location can be detected in various segmentation methods [20]. The simplest one is by trasholding the image intensity in such a way that it will capture only the fluorescent material [21]. Since the fluorescent material in cells that have pores, penetrate out, the right tuning of this threshold should be performed before the start of electroporation. Using the threshold, we can derive the cells' boundaries:

$$(\hat{x}_j, \hat{y}_j) = \operatorname{argmax}_{(x_j, y_j)} (I_{0,jL_r < r < j(L_r+1)}^{block} > Th_{I-cell}), \quad (3)$$

where the range index j moves between 1, and N , $I_{i,L < r < j(L_r+1)}^{block}$, is the intensity matrix at time instance before the electroporation starts, and at the j 'th range. Th_{I-cell} is the threshold, which is tuned in a such a way, that its related indexes, (\hat{x}_j, \hat{y}_j) , capture most of the cell areas pixels.

The cell region indexes are used for the other time instances, to mark the cells' area. For each block j 'th in time instance i 'th, the average intensity, $\mu_{i,j}^l$, is calculated along the cell surface:

$$\mu_{i,j}^l = E \left(I_{i,jL_r < r < j(L_r+1)}^{block}(\hat{x}_j, \hat{y}_j) \right). \quad (4)$$

The result in (4) is noisy due to spatial and temporal artifacts. To exclude the temporal artifacts, the intensity in (4) is normalized by an temporal normalization constant derived by the reference area outside the electroporation range, $R_2 < r$ with corresponding range indexes of j_{REF} , at instance time i :

$$\mu_{i,j}^t = \mu_{i,j}^l / \mu_{i,j_{REF}}^l. \quad (5)$$

To exclude the spatial artifacts, due to difference in cells size, location and their conductance properties variability, we will normalize the cells for each j , in their initial average intensity value, $\mu_{0,j}^l$:

$$\mu_{i,j}^{ltr} = \mu_{i,j}^t / \mu_{0,j}^l. \quad (6)$$

This data can be now stored and used as the solution to average cells' concentration in (1), at the range of jL_r in time instance i :

$$\hat{C}_{i,jL_r < r < j(L_r+1)}^l = \mu_{i,j}^{ltr}. \quad (7)$$

B. Filtering the Results Using A-priori Knowledge

To filter out results, we can exploit the continuity nature of the solution, by applying a continuity constraint. In addition, we can apply the asymptotic known properties of the solution, by matching the solution to an analytical estimation of the solution to (1).

An analytical estimation of solution can be based on matching different solutions that minimize an error criterion. A solution, must keep the asymptotic properties of the solution in (1): (a) at high time instances, there is steady state solution, and the solution does not change along different locations on the disk; (b) at very small time instances, just after the electroporation, there is still no effect on the electroporation; (c) the effect of the electroporation in ranges that are far behind the cathode is neglected.

Such a solution can be, that use a first order kinetics for pore closure similar to [22], and keep the asymptotic properties of the electroporation, can be in the form of:

$$\hat{I}_{t,r} = I_{\infty,r} e^{b(r)} e^{-\left(\frac{t}{\tau}\right)}, \quad (8)$$

where I_0 is the intensity before the electroporation, and $b(r) = 1/\ln(I_{\infty,r})$, and τ , is the pore resealing constant.

C. Estimation of the fundamental electroporation parameters

From the curves we can estimate the treatment range, electroporation areas, desired treatment time, and other parameters.

1) Electroporation effect distance

The analytical expression in (8) can be used to derive the electroporation parameters.

For instance, to estimate the effective treatment range, we look on the intensity expression from (6), or we can minimize the estimation error following analytical expression:

$$\hat{r}_0 = \operatorname{argmin}_{r_0} \left\{ \sum_{i,j} (\hat{I}_{i,jL_r}(r_0) - I_{i,j})^2 \right\}, \quad (9)$$

where $\hat{I}_{t,r}(r_0) = \begin{cases} \hat{I}_{t,r}(r_0) = I_0 & r > r_0 \\ \hat{I}_{t,r}(r_0) = \hat{I}_{t,r}(r) & \text{else} \end{cases}$, and I_0 is the maximal value of $\hat{I}_{t,r}$, which can be considered after the normalization, as 1.

2) Reversible vs. Irreversible Areas

From the intensity curves we can predict which areas of the disk have reversible, irreversible, or non-electroporation areas. Areas in which the intensity decreases to zero, all the cells have irreversible electroporation. Areas where the intensity is close to I_0 , are far behind the effect of electroporation. And areas in between, are areas where part of the cells have reversible electroporation.

3) Pores resealing constant

The pore resealing constant, τ , which is a decay constant can be derived by fitting the analytical solution in (8) to the experimental data in the effective electroporation area.

IV. EXPERIMENTAL SETUP

The experiment setup includes a fluorescent microscope (Zeiss Axiovert 200M, Carl Zeiss Micro-Imaging, Inc.), and normal human fibroblast cells cultured to 95% confluence in 35 mm petri dishes. For microscope imaging of electroporation-driven mass transports, we loaded the cells with calcein-AM orange. Three plates were used for each experimental condition. The cells were incubated with minimum essential medium (MEM) supplemented with 25mg/ml of HEPES to maintain the pH of the medium between 7.2-7.4 during the experiment.

For the electroporation, we applied 50 pulses with 750 V on the central electrode the external electrode was grounded. The applied pulsed duration was 70 μ s and pulses were delivered at 1 Hz.

The images were taken highest intensity with minimum saturation, to ensure maximal pixel resolution. Since the intensity decreases after electroporation, over time, to maximize the dynamic range and fluorophore bleaching, we tuned the peak areas with the highest intensity to reach the saturated value. The exposure time 600 μ s was constant throughout the total imaging duration of 80 minutes. We also took into account the effect of fluorophore bleaching by studying a non-electroporated area on each disk.

V. RESULTS

Figure 2, shows the selected electroporation area, and the reference area, right after the electroporation, when there is still no effect, and after 80 minutes, where the effect is clear. It can be seen, that the area outside of the anode, is unaffected. Still, it is hard to quantify the electroporation parameters just by these figures.

Figure 3, shows the cell estimated region, after applying the threshold in (3). It seems that most of the cell surface is captured, and that the images are synchronized in time. The mean value of these surfaces in (4) is used to approximate the average cells concentration in the block.

The results in time-space domains and after exclusion of temporal artifacts by normalization to the value at the first time instance, and after spatial artifact exclusion by using the reference area in Figure 2, are shown in Figure 4.a-c. Figure 4.d, show the analytical estimation results that filter out some of the spatio-temporal noise effects by applying the a-priori

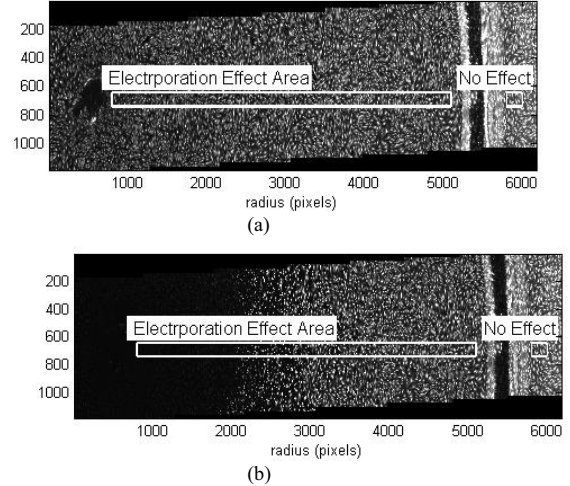


Fig. 2. Figure 2.a, describes the selected electroporation and reference areas just after the electroporation. The left black and right black areas are the areas of the cathode, and anode, respectively. Figure 2.b, describes the same area, after 80 minutes. The black area near the cathode is of cells with irreversible electroporation, whose fluorescent content was diffused out of the cell.

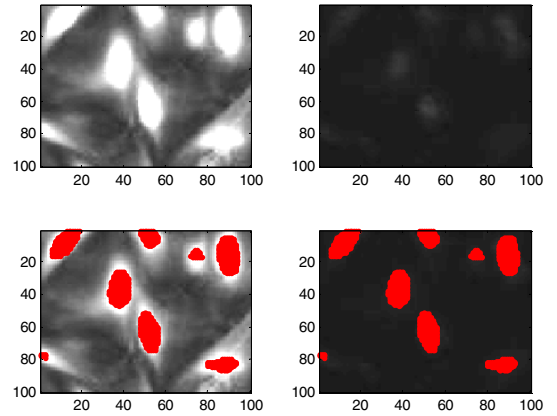


Fig. 3. The selected cells are marked by red. The left figure shows the area near the cathode just after the electroporation. The cells areas are used to estimate the cell location, and to estimate the average cells' concentration over time. The right figure shows the same block after 80 minutes.

knowledge about maximal intensity values, and about asymptotic conditions. It seems that the estimation captures most of the intensity properties, and furthermore smooth the results in (6). The average estimation error is less than 3%, and the electroporation effective range r_0 is 3.5 mm, from the cathode. Furthermore, the electroporation user, by using the estimation, can use only part of the data set obtained after short time, and deduce the rest of the curve. This can speed up the whole analysis process.

Figure 5, shows how the different areas of electroporation can be distinguished by simple observation of the electroporation intensity plot.

VI. CONCLUSIONS AND FUTURE WORK

We suggested in this work a new procedure to ease the tedious procedure that is required today for electroporation

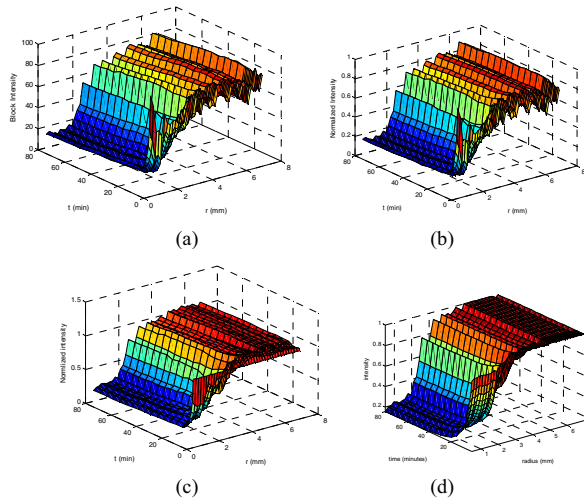


Fig. 4. The different post processing stages. Figure 4.a, Figure 4.b, and Figure 4.c, show the results of intensity before post processing, after temporal artifacts exclusion, and after spatial artifact exclusion, respectively. Figure 4.d shows the analytical function approximation after aggregating a-priori knowledge.

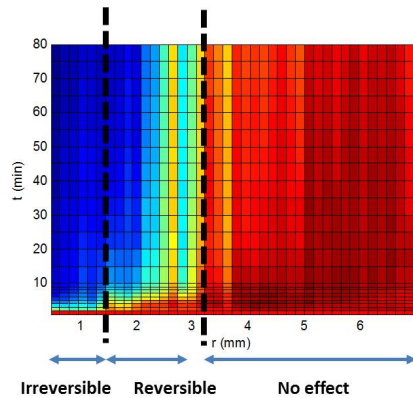


Fig. 5. From the graph we can obtain the areas of non, reversible, and irreversible electroporation areas.

users, without scarifying in estimation accuracy. Using the new methods include analytical estimation after aggregating a-priori knowledge about maximal intensity value, we can use only one data set of the results, and give accurate results with only one experiment. In addition, due to the new experiment setup, the suggested system can enable the extraction of multiple electroporation parameters in a single experiment.

Future work is to derive an accurate analytical expression, for clinical relevant cell lines, which includes aggregation of a-priori knowledge and will enable to estimate more parameters that are related to electroporation, and to produce automated ways to derive the different electroporation areas.

REFERENCES

[1] E. Neumann, A. E. Sowers, and C. A. Jordan, *Electroporation and electrofusion in cell biology*: Springer, 1989.
 [2] A. Golberg, Y. Fischer, and B. Rubinsky, "The Use of Irreversible Electroporation in Food Preservation," in *Irreversible Electroporation*, B. Rubinsky, Ed., ed Chennai Springer, 2010, pp. 273–312.

[3] A. Golberg and M. L. Yarmush, "Nonthermal irreversible electroporation: fundamentals, applications, and challenges," *IEEE Trans Biomed Eng*, vol. 60, pp. 707–14, Mar 2013.
 [4] E. Neumann, M. Schaefer-Ridder, Y. Wang, and P. H. Hofschneider, "Gene transfer into mouse lyoma cells by electroporation in high electric fields," *EMBO Journal*, vol. 1, pp. 841–845, 1982.
 [5] L. M. Mir, M. Belehradek, C. Domenge, S. Orlowski, B. Poddevin, J. Belehradek, Jr., G. Schwaab, B. Lubinski, and C. Paoletti, "[Electrochemotherapy, a new antitumor treatment: first clinical trial]," *C R Acad Sci III*, vol. 313, pp. 613–8, 1991.
 [6] M. Okino and H. Mohri, "Effects of a high-voltage electrical impulse and an anticancer drug on in vivo growing tumors," *Japanese journal of cancer research : Gann*, vol. 78, pp. 1319–21, Dec 1987.
 [7] S. Orlowski, J. Belehradek, Jr., C. Paoletti, and L. M. Mir, "Transient electroporation of cells in culture. Increase of the cytotoxicity of anticancer drugs," *Biochem Pharmacol*, vol. 37, pp. 4727–33, Dec 15 1988.
 [8] A. I. Daud, R. C. DeConti, S. Andrews, P. Urbas, A. I. Riker, V. K. Sondak, P. N. Munster, D. M. Sullivan, K. E. Ugen, J. L. Messina, and R. Heller, "Phase I trial of interleukin-12 plasmid electroporation in patients with metastatic melanoma," *Journal of Clinical Oncology*, vol. 26, pp. 5896–903, Dec 20 2008.
 [9] A. V. Titomirov, S. Sukharev, and E. Kistanova, "In vivo electroporation and stable transformation of skin cells of newborn mice by plasmid DNA," *Biochimica et biophysica acta*, vol. 1088, pp. 131–4, Jan 17 1991.
 [10] R. Davalos, L. M. Mir, and B. Rubinsky, "Tissue Ablation with Irreversible Electroporation," *Annals of Biomedical Engineering*, vol. 33, pp. 223–231, 2005.
 [11] A. Golberg, M. Belkin, and B. Rubinsky, "Irreversible electroporation for microbial control of drugs in solution," *AAPS PharmSciTech*, vol. 10, pp. 881–6, 2009.
 [12] A. Golberg, C. S. Rae, and B. Rubinsky, "Listeria monocytogenes cell wall constituents exert a charge effect on electroporation threshold," *Biochimica et Biophysica Acta (BBA) - Biomembranes*, vol. 1818, pp. 689–694, 2012.
 [13] G. Pucihar, J. Krmelj, M. Rebersek, T. B. Napotnik, and D. Miklavcic, "Equivalent pulse parameters for electroporation," *IEEE Trans Biomed Eng*, vol. 58, pp. 3279–88, Nov 2011.
 [14] F. Fernand, L. Rubinsky, A. Golberg, and B. Rubinsky, "Variable electric fields for high throughput electroporation protocol design in curvilinear coordinates," *Biotechnol Bioeng*, vol. 109, pp. 2168–71, 2012.
 [15] O. Dzyubachyk, W. Niessen, and E. Meijering, "Advanced level-set based multiple-cell segmentation and tracking in time-lapse fluorescence microscopy images," in *Biomedical Imaging: From Nano to Macro, 2008. ISBI 2008. 5th IEEE International Symposium on*, 2008, pp. 185–188.
 [16] M.-P. Rols and J. Teissie, "Electroporation of mammalian cells. Quantitative analysis of the phenomenon," *Biophysical journal*, vol. 58, pp. 1089–1098, 1990.
 [17] W. Krassowska and P. D. Filev, "Modeling electroporation in a single cell," *Biophys J*, vol. 92, pp. 404–17, Jan 15 2007.
 [18] Y. Granot and B. Rubinsky, "Mass Transfer Model for Drug Delivery in Tissue Cells with Reversible Electroporation," *International Journal of Heat and Mass Transfer*, vol. 51, pp. 5610–5616, 2008.
 [19] A. Golberg and B. Rubinsky, "A statistical model for multidimensional irreversible electroporation cell death in tissue," *Biomed Eng Online*, vol. 9, pp. 9–13, 2010.
 [20] A. Dufour, V. Shinin, S. Tajbakhsh, N. Guillén-Aghion, J.-C. Olivio-Marin, and C. Zimmer, "Segmenting and tracking fluorescent cells in dynamic 3-D microscopy with coupled active surfaces," *Image Processing, IEEE Transactions on*, vol. 14, pp. 1396–1410, 2005.
 [21] M. E. Sieracki, S. E. Reichenbach, and K. L. Webb, "Evaluation of automated threshold selection methods for accurately sizing microscopic fluorescent cells by image analysis," *Applied and Environmental microbiology*, vol. 55, pp. 2762–2772, 1989.
 [22] G. Blumrosen and A. Freedman, "Sensitivity study and a practical algorithm for ml ostbc and beam forming combination," in *The 23rd IEEE Convention of Electrical and Electronics Engineers in Israel*, 2004.